

Wave-front estimation from wave-front slope measurements

W. H. Southwell

Rockwell International Corporation, Rocketdyne Division, Canoga Park, California 91304

(Received 28 August 1979; revised 21 February 1980)

The problem of wave-front estimation from wave-front slope measurements has been examined from a least-squares curve fitting model point of view. It is shown that the slope measurement sampling geometry influences the model selection for the phase estimation. Successive over-relaxation (SOR) is employed to numerically solve the exact zonal phase estimation problem. A new zonal phase gradient model is introduced and its error propagator, which relates the mean-square wave-front error to the noisy slope measurements, has been compared with two previously used models. A technique for the rapid extraction of phase aperture functions is presented. Error propagation properties for modal estimation are evaluated and compared with zonal estimation results.

INTRODUCTION

In this paper we consider the problem of estimating wave-front phase from a set of discrete phase slope measurements. This reconstruction process is necessary to obtain phase profile estimates from certain types of sensors, such as a shearing interferometer or a Hartmann sensor. It is also necessary in image restoration using the Knox-Thompson¹ speckle imaging technique.

A variety of approaches have been proposed to accomplish this phase reconstruction. Basically, each estimation approach may be categorized as being either zonal or modal depending on whether the estimate is a phase value in a local zone or a coefficient of an aperture function. In either case, least-squares estimation is used for the phase reconstruction.

Differences in the methods can be distinguished by the different models used to "fit" the local slope measurements.

Some important considerations in selecting a model are (i) compatibility; does the model fit the geometry of the slope measurements as given by the sensor?, (ii) numerical complexity; are there convergence problems, storage, and computation speed requirements?, and (iii) error propagation; what effect does noise in the slope measurements have on the phase estimates?

The reconstruction problem was first addressed in the literature by Rimmer,² and since then by a number of authors.³⁻⁸ Most of these papers use a phase difference slope model for zonal reconstruction that is chiefly applicable to a shearing interferometric sensor, where the x -slope measurement positions are not coincident with the y -slope measurement po-

sitions. With some approximations, Hudgin³ calculated the noise propagator for this model. Using a model that assumed coincident x - and y -slope measurements and some approximations, Fried⁴ also calculated the noise propagation parameter. Recently, Herrmann⁸ constructed an exact solution for the noise propagator for the models of both Fried and Hudgin. Herrmann's results essentially confirmed the previous results.

In this paper we present a new phase reconstruction model which, like that of Fried is applicable to coincident x - and y -slope measurements (and thus suitable for Hartmann sensors). The error propagation properties of this new model have been shown to be superior to the models of both Hudgin and Fried, partly because it provides a more uniform sampling of the aperture. We also describe, and illustrate with examples, a matrix iterative technique that solves the exact least-squares zonal reconstruction problem, is easy to implement, and exhibits rapid convergence.

Modal estimation is also discussed. Some numerical methods for the rapid extraction of the low-order orthogonal modes are described. Finally, noise propagation effects using modal estimation are compared with those using zonal estimation.

ZONAL ESTIMATION

Three grid configurations that illustrate the grid positions for the x - and y -slope measurements and the reconstructed phases are shown in Fig. 1. It is important to point out that the formulation of the problem depends on the grid pattern used, which, in turn, depends on where the actual slope measurements are taken. Figure 1(A) would be applicable, for example, for a Hartmann sensor, where each small lens mea-

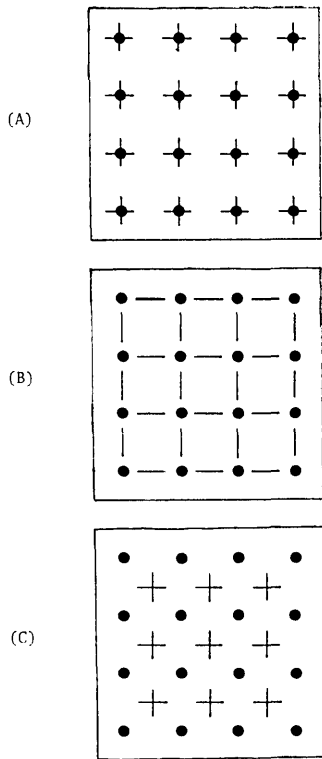


FIG. 1. Slope measurement sampling geometry and wavefront mesh points. The horizontal dashes indicate positions of x -slope sampling. The vertical dashes are the y -slope sampling positions. The dots are the estimated phase points. Configuration B has been considered previously by Hudgin and configuration C by Fried.

$$S_{ij}^y = (\phi_{i,j+1} - \phi_{ij})/h \quad \begin{matrix} i = 1, N \\ j = 1, N - 1 \end{matrix}, \quad (6)$$

where $h = D/N$ and D is the width of the aperture. Each phase point represents an equal subregion of area h^2 in the aperture. This is the least-squares model used by Hudgin.³ (We note that it is equivalent to the assumption of a bilinear spline phase on the phase grid of Fig. 1(B). The phase is everywhere continuous, but has discontinuous slopes at the mesh points.)

It is also interesting to note that we have derived the slope model based on actual local slopes. But we see from Eqs. (5) and (6) that the model is equally applicable to the assumption that the slopes be determined by adjacent phase differences.

Now suppose our x - and y -slope measurements are given at coincident points, as in a Hartmann sensor plate. One possibility is to let the phase points used in Eq. (4) be replaced by the average of two phase values which are positioned perpendicular to the slope direction by one half-step up and one half-step down. This is the configuration shown in Fig. 1(C). This gives the slope model used by Fried,⁴

$$S_{ij}^x = \frac{[(\phi_{i+1,j} + \phi_{i+1,j+1})/2 - (\phi_{ij} + \phi_{i,j+1})/2]}{h}, \quad (7)$$

$$S_{ij}^y = \frac{[(\phi_{i,j+1} + \phi_{i+1,j+1})/2 - (\phi_{ij} + \phi_{i+1,j})/2]}{h}. \quad (8)$$

For a new model appropriate for Hartmann sensor measurements, we consider the grid geometry of Fig. 1(A) and return to Eqs. (1) and (2) for a representation of the phase between mesh points. This time we have two measurements per interval, a slope at each end. This enables the determination of both c_1 and c_2 in Eq. (2).

This produces the relationships

$$\frac{(S_{i+1,j}^x + S_{ij}^x)}{2} = \frac{(\phi_{i+1,j} - \phi_{ij})}{h} \quad \begin{matrix} i = 1, N - 1 \\ j = 1, N \end{matrix}, \quad (9)$$

$$\frac{(S_{i+1,j}^y + S_{ij}^y)}{2} = \frac{(\phi_{i,j+1} - \phi_{ij})}{h} \quad \begin{matrix} i = 1, N \\ j = 1, N - 1 \end{matrix}. \quad (10)$$

[We comment that the phase model used for data configuration like Fig. 1(A) is a biquadratic spline, whereas configurations like Fig. 1(B) are based on a bilinear spline phase. However, since we are not interpolating, but only determining the phase at the mesh points, it does not necessarily mean that one is more accurate in the phase estimation.]

LEAST-SQUARES SOLUTION

Having a set of measurements S^x and S^y and a model for these quantities [Eqs. (5) and (6), (7) and (8), or (9) and (10) in terms of the adjustable parameters ϕ_{ij}], it is straightforward to apply least-squares techniques. However, there are some potential difficulties which require attention.

To formulate the least-squares problem, note that Eqs. (5) and (6) or Eqs. (7) and (8) may be written as a single matrix equation

$$\mathbf{S} = \mathbf{A}\phi, \quad (11)$$

where \mathbf{S} is a vector containing all the slope measurements (x

sures both the x and y slopes at the same point. Figure 1(B) could be applicable, for example, in a shearing interferometer where the beam is first divided in order to apply, separately, the x and y shears. Figure 1(C) shows coincident x and y slopes, but with a displaced phase grid.

The problem is to least-squares-fit the slope measurement data to some function or model of the phase given at its grid points. Consider first the data configuration given in Fig. 1(B). In that configuration there are N^2 phase points and $2N(N-1)$ slope measurement points. Let us assume that the phase dependence between grid points in the x direction is represented by the polynomial

$$\phi = c_0 + c_1x + c_2x^2. \quad (1)$$

The slope is

$$S^x = c_1 + 2c_2x. \quad (2)$$

But since we have only one slope measurement, which is given at the midpoint of the interval, we can only determine c_1 . The constant c_0 is the value of the phase at the left side of the interval. Thus, all that the data can support is a linear phase model,

$$\phi = \phi_i + S_i^x x. \quad (3)$$

The phase at the right of the interval ($x = h$) is ϕ_{i+1} . Applying this boundary fact leads to the slope model,

$$S_i^x = (\phi_{i+1} - \phi_i)/h \quad i = 1, N - 1, \quad (4)$$

where N is the number of phase sample points in the x direction. Generalizing to all rows and to the y direction, we obtain,

$$S_{ij}^x = (\phi_{i+1,j} - \phi_{ij})/h \quad \begin{matrix} i = 1, N - 1 \\ j = 1, N \end{matrix}, \quad (5)$$

slopes first) and ϕ is a vector of length N^2 containing all the unknown phase values. The size of the rectangular matrix \mathbf{A} is N^2 by the number of slope measurements; however, it is very sparse. Multiplying Eq. (14) from the left by \mathbf{A}^\dagger (\mathbf{A} transpose), we obtain the normal equations

$$(\mathbf{A}^\dagger \mathbf{A})\phi = \mathbf{A}^\dagger \mathbf{S}, \quad (12)$$

which are a set of N^2 linear equations in N^2 unknowns ϕ_{jk} . The standard least-squares solution is obtained by multiplying the right-hand side of Eq. (12) by the inverse of the square matrix $\mathbf{A}^\dagger \mathbf{A}$.

However, the standard least-squares solution cannot be used because $\mathbf{A}^\dagger \mathbf{A}$ is singular. This is a consequence of the fact that any constant wave front added to the correct wave front also satisfies the models. This does not mean that Eq. (12) cannot be solved for a meaningful solution. But it does mean we cannot use the standard matrix inversion technique.

Herrmann has shown that the desired solution is the one that has a minimum norm, which has zero mean. He shows that using the zero-mean condition leads to an extended \mathbf{A}_e matrix that yields an $\mathbf{A}_e^\dagger \mathbf{A}_e$ matrix that is not singular. The matrix \mathbf{A}_e has an additional row (of all ones) and \mathbf{S}_e has an additional element (zero). However, this procedure requires the computer storage of a matrix the size \mathbf{A} , which has essentially $2N^2$ elements.

For large arrays, we can use iterative matrix methods for solving Eq. (12). The solution obtained is unique to within an additive constant, but it is an easy matter to subtract out the mean. We discuss these methods below. But first, we write the matrix equation representing Eqs. (9) and (10), the Fig. 1(A) model,

$$\mathbf{D}\mathbf{S} = \mathbf{A}\phi, \quad (13)$$

where \mathbf{D} is a large sparse matrix that performs the adjacent slope averaging. The corresponding normal equations are

$$(\mathbf{A}^\dagger \mathbf{A})\phi = \mathbf{A}^\dagger \mathbf{D}\mathbf{S}. \quad (14)$$

MATRIX ITERATIVE SOLUTIONS

For large arrays, we can take advantage of the sparse nature of $\mathbf{A}^\dagger \mathbf{A}$ and use matrix iterative methods for solving Eqs. (12) and (14). If we write just the nonzero matrix element components of Eq. (12) for Fig. 1(B) configuration, we obtain

$$g_{jk} \phi_{jk} - [\phi_{j+1,k} + \phi_{j-1,k} + \phi_{j,k+1} + \phi_{j,k-1}] = [S_{j,k-1}^y - S_{jk}^y + S_{j-1,k}^x - S_{jk}^x] h, \quad (15)$$

where

$$g_{jk} = \begin{cases} 2 & j = 1 \text{ or } N; k = 1 \text{ or } N \\ 3 & \begin{cases} j = 1 \text{ or } N; k = 2 \text{ to } N-1 \\ k = 1 \text{ or } N; j = 2 \text{ to } N-1 \end{cases} \\ 4 & \text{otherwise,} \end{cases} \quad (16)$$

and if a nonexistent matrix element is called for, then zero is assumed. The g factors are the diagonal elements of $\mathbf{A}^\dagger \mathbf{A}$, which are either 2, 3, or 4 according to whether its accompanying phase point ϕ_{jk} is on a corner, an edge, or an interior point. Calling the right-hand side b_{jk} , we can rewrite Eq. (15) as

$$\phi_{jk} = \bar{\phi}_{jk} + b_{jk}/g_{jk}, \quad (17)$$

where $\bar{\phi}_{jk}$ is the nearest-neighbor phase average,

$$\bar{\phi}_{jk} = [\phi_{j+1,k} + \phi_{j-1,k} + \phi_{j,k+1}]/g_{jk}, \quad (18)$$

and

$$b_{jk} = [S_{j,k-1}^y - S_{jk}^y + S_{j-1,k}^x - S_{jk}^x]h, \quad (19)$$

which is a constant depending only on the slope measurements.

Equation (17) forms the basis for an iterative solution. The right-hand side of Eq. (17) is evaluated using current values for the ϕ 's (which may initially be zero). The result becomes the improved estimate; at the m th iteration, this becomes

$$\phi_{jk}^{(m+1)} = \bar{\phi}_{jk}^{(m)} + b_{jk}/g_{jk}. \quad (20)$$

If the left-hand side is held in a separate array until all N^2 points are evaluated, then this procedure is the Jacobi method. If, however, the left-hand side updates the wave-front array directly, such that succeeding evaluations of the right-hand side could use phase points that have already been updated, then the procedure is called the Gauss-Seidel method. Generally, the Gauss-Seidel method converges faster and is easier to implement.

Neither of these methods, however, updates a phase point based on the previous value at that point, since $\bar{\phi}_{jk}$ does not include ϕ_{jk} .

By adding and subtracting ϕ_{jk} on the right-hand side of Eq. (20) and introducing the relaxation parameter ω , we have

$$\phi_{jk}^{(m+1)} = \phi_{jk}^{(m)} + \omega [\bar{\phi}_{jk}^{(m)} + b_{jk}/g_{jk} - \phi_{jk}^{(m)}]. \quad (21)$$

This iterative technique is the successive over-relaxation (SOR) method. Convergence is achieved when the quantity in brackets on the right-hand side becomes small. The SOR method generally promises improvement in convergence; however, it is necessary to determine the value of the relaxation parameter ω which maximizes the rate of convergence.

Fortunately, $\mathbf{A}^\dagger \mathbf{A}$ for the phase reconstruction problem belongs to a class of matrices for which the optimal value of ω is known.⁹ The result is

$$\omega = \frac{2}{1 + \sin[\pi/(N+1)]}. \quad (22)$$

The results of a numerical comparison of the three matrix iteration methods discussed above are tabulated in Table I. The slope measurements were generated from the analytical derivatives of a simulated wave front, which in this example contained astigmatism. The rms wave-front reconstruction error was calculated by comparing the wave front reconstructed from the slopes with the simulated wave front. The Jacobi method converged but left a small residual error in this example, although it generally gives the correct answer. The Gauss-Seidel method converged in approximately N^2 iterations, whereas the SOR method converged in approximately $2N$ iterations. (An analysis of the convergence rates indicates that for large N , SOR will converge $2N/\pi$ fewer iterations than the Gauss-Seidel method.)

Hudgin³ formulates the wave-front reconstruction problem in such a way that edge effects are ignored. They deal with Eq. (15) where all the $g_{jk} = 4$, which treats all phase points as

TABLE I. rms wave-front reconstruction error in waves as a function of the number of iterations for three different iterative methods. The sampled wave front contained astigmatism of the form $W = 2.3717(x^2 - y^2)/a^2 + 6xy/a^2$ over a square aperture of area $4a^2$.

| Number of iterations | Jacobi | Gauss-Seidel | SOR | N |
|----------------------|--------|--------------------|--------------------|-----|
| 2 | 0.487 | 0.504 | 0.620 | 4 |
| 4 | 0.176 | 0.255 | 0.249 | |
| 8 | 0.126 | 0.043 | 2×10^{-4} | |
| 16 | 0.125 | 8×10^{-4} | 0 | |
| 32 | 0.125 | 3×10^{-7} | 0 | |
| 64 | 0.125 | 0 | 0 | |
| 2 | 1.638 | 1.389 | 1.062 | 8 |
| 4 | 1.288 | 0.936 | 0.664 | |
| 8 | 0.823 | 0.454 | 0.319 | |
| 16 | 0.350 | 0.151 | 0.022 | |
| 32 | 0.067 | 0.034 | 6×10^{-5} | |
| 64 | 0.014 | 0.002 | 0 | |
| 128 | 0.013 | 4×10^{-6} | 0 | |
| 256 | 0.013 | 0 | 0 | |
| 2 | 2.068 | 1.963 | 1.563 | 16 |
| 4 | 1.947 | 1.763 | 1.159 | |
| 8 | 1.744 | 1.446 | 0.716 | |
| 16 | 1.422 | 0.996 | 0.344 | |
| 32 | 0.969 | 0.492 | 0.046 | |
| 64 | 0.467 | 0.135 | 5×10^{-4} | |
| 128 | 0.113 | 0.022 | 0 | |
| 256 | 0.007 | 0.001 | 0 | |
| 512 | 0.002 | 6×10^{-6} | 0 | |
| 1024 | 0.002 | 0 | 0 | |

being in the interior of the aperture. Such an assumption can lead to large wave-front reconstruction errors. Table II shows the wave-front reconstruction results using the recursive algorithm of Hudgin on the same slope data used in Table I. The large errors indicate that the simulated wave front was not reconstructed. This means that edge effects are important—even for $N = 16$, where nearly one-fourth of the phase points lie on the aperture edge.

Frost *et al.*⁷ also neglect edge effects in order to utilize a fast-Fourier-transform solution method. The results of their numerical examples appear to be quite good; however, they used a large phase grid, $N = 256$.

For practical wave-front sensors, where N will probably be less than 35, the aperture boundary or edge effects are important. To make this point more explicit, we used the recursive algorithm of Hudgin on a simulated wave front with defocus $W = 1.732[2(x^2 + y^2) - 1]$. Using an $N = 4$ grid, the correct wave front is

$$\phi = \begin{pmatrix} 2.17 & 0.43 & 0.43 & 2.17 \\ 0.43 & -1.30 & -1.30 & 0.43 \\ 0.43 & -1.30 & -1.30 & 0.43 \\ 2.17 & 0.43 & 0.43 & 2.17 \end{pmatrix}. \quad (23)$$

The exact analytical derivatives were used to generate the slope data at the midpoints between sample points. The reconstructed wave front, using the recursive formula of Hudgin, gave the following result (after applying an unimportant constant offset of 1.588):

$$\hat{\phi} = \begin{pmatrix} 2.17 & 1.01 & 1.01 & 2.17 \\ 1.01 & -0.72 & -0.72 & 1.01 \\ 1.01 & -0.72 & -0.72 & 1.01 \\ 2.17 & 1.01 & 1.01 & 2.17 \end{pmatrix}. \quad (24)$$

The rms wave-front reconstruction error was 0.25 waves.

We next write the nonzero matrix element components of Eq. (14), Fig. 1(A) configuration:

$$g_{jk}\phi_{jk} - [\phi_{j+1,k} + \phi_{j-1,k} + \phi_{j,k+1} + \phi_{j,k-1}] = \frac{1}{2} [S_{j,k+1}^y - S_{j,k-1}^y + S_{j+1,k}^x - S_{j-1,k}^x] h, \quad (25)$$

where

$$g_{jk} = \begin{cases} 2 & j = 1 \text{ or } N; k = 1 \text{ or } N \\ 3 & \begin{cases} j = 1 \text{ or } N; k = 2 \text{ to } N - 1 \\ k = 1 \text{ or } N; j = 2 \text{ to } N - 1 \end{cases} \\ 4 & \text{otherwise,} \end{cases} \quad (26)$$

and if a nonexistent phase element is called for, then zero is assumed, and if a nonexistent slope element is called for, then the negative of the adjacent slope is assumed. The only difference between this equation and Eq. (15) is in the formation of the right-hand side of Eq. (25), which is only a manipulation of the data. Consequently, the same SOR technique, Eq. (21), may be applied, except that b_{jk} is now the right-hand side of Eq. (25).

ZONAL ESTIMATION ERROR

There are two important sources of error in the reconstruction process. One is the algorithm accuracy. That is, how well does the least-squares process reconstruct a phase of arbitrary shape? The answer, of course, depends on the shape of the wave front being measured. For example, numerical experimentation indicates that the zonal reconstruction models discussed here will perfectly reconstruct

TABLE II. Wave-front reconstruction results using the recursive formula of Hudgin (which neglects edge effects). Shown here is the rms wave-front reconstruction error in waves from slope data sampled from a wave front containing astigmatism of the form $W = 2.3717(x^2 - y^2)/a^2 + 6xy/a^2$ over a square aperture of area $4a^2$. In each case the recursive algorithm quickly converged, but did not reproduce the sampled wave front.

| Number of iterations | rms error | N |
|----------------------|-----------|-----|
| 2 | 1.106 | 4 |
| 4 | 1.158 | |
| 8 | 1.160 | |
| 16 | 1.159 | |
| 2 | 1.624 | 8 |
| 4 | 1.602 | |
| 8 | 1.625 | |
| 16 | 1.624 | |
| 2 | 1.944 | 16 |
| 4 | 1.905 | |
| 8 | 1.897 | |
| 16 | 1.908 | |

wave fronts having any combination of tilts, defocus, and astigmatism. Furthermore, this is true for any N . However, for wave fronts with higher-order aberrations, the model gives nonperfect reconstruction that is N dependent. Basically, this type of error is a consequence of the finite sampling density.

The other important source of error is that produced from noise in the slope measurements.

The basis for determining the error propagation, that is, the amount of error resulting from errors in the slope measurements, is given by the model itself, or the normal equations, Eq. (12) [or Eq. (14)]:

$$(\mathbf{A}_e^\dagger \mathbf{A}_e) \phi = \mathbf{A}^\dagger \mathbf{S}, \quad (27)$$

where we now use the extended matrix \mathbf{A}_e (discussed above) to assure that our solutions will have zero mean. We assume now that our slope measurements contain random additive noise,

$$\mathbf{S} = \mathbf{S}_0 \pm \sigma. \quad (28)$$

We now ask, what is ϵ , the resulting error in wave front ϕ ? To answer this, write

$$\phi = \phi_0 \pm \epsilon, \quad (29)$$

and apply the linear relationship Eq. (27). We obtain

$$(\mathbf{A}_e^\dagger \mathbf{A}_e) (\phi_0 \pm \epsilon) = \mathbf{A}^\dagger (\mathbf{S}_0 \pm \sigma), \quad (30)$$

$$(\mathbf{A}_e^\dagger \mathbf{A}_e) \epsilon = \mathbf{A}^\dagger \sigma, \quad (31)$$

since \mathbf{S}_0 and ϕ_0 are assumed to be the true values. Thus, the wave-front errors ϵ will obey the same set of normal equations that the wave front obeys. Furthermore, the new $\mathbf{A}_e^\dagger \mathbf{A}_e$ matrix is not singular. This permits, in principle at least, the application of the standard linear least-squares solution

$$\epsilon = \mathbf{B} \sigma, \quad (32)$$

where

$$\mathbf{B} = (\mathbf{A}_e^\dagger \mathbf{A}_e)^{-1} \mathbf{A}^\dagger \quad (33)$$

or

$$\mathbf{B} = (\mathbf{A}_e^\dagger \mathbf{A}_e)^{-1} \mathbf{A}^\dagger \mathbf{D}, \quad (34)$$

where Eq. (34) is applicable for the model in Fig. 1(A).

A particular phase error component is

$$\epsilon_i = \sum_k B_{ik} \sigma_k. \quad (35)$$

We next form the product $\epsilon_i \epsilon_j$ and take the statistical average,

$$\langle \epsilon_i \epsilon_j \rangle = \sum_k \sum_l B_{ik} B_{jl} \langle \sigma_k \sigma_l \rangle; \quad (36)$$

but since the slope errors are independent and uncorrelated (and, we assume, equal),

$$\langle \sigma_k \sigma_l \rangle = \sigma^2 \delta_{kl}. \quad (37)$$

Equation (36) becomes

$$\langle \epsilon_i \epsilon_j \rangle = \sigma^2 \sum_k B_{ik} B_{jk}, \quad (38)$$

$$= \sigma^2 [\mathbf{B}\mathbf{B}^\dagger]_{ij}. \quad (39)$$

The matrix on the right-hand side of Eq. (39) is not diagonal, which means that the phase errors are not uncorrelated. Nor are the phase errors equal at each point.

To obtain the mean-square phase error E , we set $i = j$ in Eq. (38) [or Eq. (39)] and average over i ,

$$E = \frac{1}{N^2} \sum_i \langle \epsilon_i^2 \rangle \quad (40)$$

$$= \frac{\sigma^2}{N^2} \sum_i \sum_k B_{ik}^2. \quad (41)$$

This says that the mean-square phase error is proportional to the sum of the square of each component of the \mathbf{B} matrix. The matrix \mathbf{B} is the same size as \mathbf{A}^\dagger but it is not sparse.

For the slope models that we considered, the matrix \mathbf{A} is fixed for a given N , except for h , the phase point separation. But since it enters in a multiplicative manner, it is easy to factor it out of the right-hand side of Eq. (41),

$$E = C h^2 \sigma^2, \quad (42)$$

where the noise coefficient C is defined by

$$C = \frac{1}{D^2} \sum_i \sum_k B_{ik}^2. \quad (43)$$

There is another way to evaluate the noise coefficient. Using the fact that the slope measurement errors are uncorrelated, the total wave-front variance will be the sum of the wave-front variances due to each slope variance separately. To show this, we assume each slope variance σ_k^2 is different and use Eq. (36) and (37) in (40),

$$E = \sum_k E_k, \quad (44)$$

where

$$E_k = \frac{1}{N^2} \sum_i B_{ik}^2 \sigma_k^2, \quad (45)$$

where, due to the independence of the σ_k , all the cross terms vanish. The scalar quantity E_k is the mean-square wave front resulting from a set of zero slopes except for σ_k . The SOR method, Eq. (21), may be used to calculate E_k . When using Eq. (21), which is based on the standard normal equations, it is important to subtract out the mean. This approach is a means of calculating the elements of \mathbf{B} without forming an inverse of $\mathbf{A}_e^\dagger \mathbf{A}_e$. The wave-front solution of Eq. (21), when all slopes are zero except σ_k (which is unity), becomes the k th column of the \mathbf{B} matrix. This is evident from Eq. (35). (This technique is similar to the approach used by Fried.⁴)

To compare our results with those previously published for phase difference measurements, we need to convert our slope errors σ to phase difference errors σ_{pd} . We do this using the expression

$$\phi_{pd} = (2\pi/\lambda)hs, \quad (46)$$

where ϕ_{pd} is the phase difference measurement associated with the slope angle s , h is the spacing, and λ is the wavelength. This gives

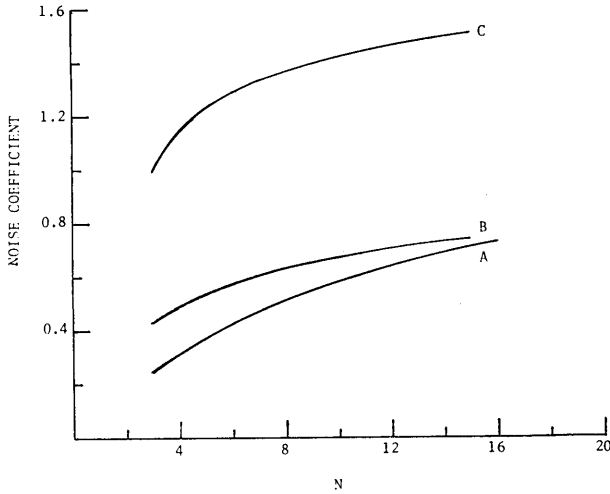


FIG. 2. Noise coefficient for zonal estimation versus N for a square array containing N^2 phase points. Curves A, B, and C correspond to the sampling geometries in Fig. 1.

$$C_{pd} = CN^2/D^2 = C/h^2, \quad (47)$$

where C_{pd} is the noise coefficient for phase difference measurements defined by

$$\langle (\delta\Phi)^2 \rangle = C_{pd} \sigma_{pd}^2, \quad (48)$$

where $\langle (\delta\Phi)^2 \rangle$ is the mean-square phase error and σ_{pd}^2 is the variance of each phase difference measurement. For all the data plotted in this paper, the noise coefficient is given by the right-hand side of Eq. (47).

We have numerically evaluated the error propagator for each configuration shown in Fig. 1. The results are shown in Fig. 2. Our results for Figs. 1(B) and 1(C) are in agreement with Herrmann.⁸ We note that the noise coefficient is lower for the data configuration of Fig. 1(A).

MODAL ESTIMATION

For comparison purposes, we assume we have the same set of slope measurements as depicted in Fig. 1. We now use these measurements to fit the coefficients in a phase expansion of orthogonal functions

$$\phi(x,y) = \sum_{k=0}^M a_k n_k F_k(x,y), \quad (49)$$

where a_k are the coefficients to be determined, n_k are the normalization constants, and F_k are the two-dimensional functions that are orthogonal over the discretely sampled aperture. For later convenience, we choose F_k to have zero mean and to be normalized such that the phase variance is

$$\sigma_\phi^2 = \sum_{k=1}^M a_k^2. \quad (50)$$

We have constructed a set F_k from products of Legendre polynomials that have the required properties

$$n_k n_l \sum_{i=1}^N \sum_{j=1}^N F_k(x_i, y_j) F_l(x_i, y_j) = N^2 \delta_{kl}, \quad (51)$$

where we have assumed that the origin of the coordinate system is at the center of the square array. We list the first 10 of these functions and their normalization constants in Table III.

The slope model is obtained by differentiating Eq. (49),

$$S^x = \sum_{k=1}^M a_k n_k \frac{\partial F_k}{\partial x}, \quad (52)$$

$$S^y = \sum_{k=1}^M a_k n_k \frac{\partial F_k}{\partial y}. \quad (53)$$

In this case, it is the M phase expansion coefficients a_k that are the adjustable parameters, instead of N^2 phase points. This greatly reduces the numerical complexity of the estimation. The partial derivatives are analytical derivatives and are also shown in Table III.

Writing Eqs. (55) and (56) in matrix form, we have

$$\mathbf{S} = \mathbf{A}\mathbf{a}, \quad (54)$$

where \mathbf{A} is a rectangular matrix with M columns and $2N^2$ rows for Fig. 1(A), $2N(N-1)$ rows for Fig. 1(B), and $2(N-1)^2$ rows for Fig. 1(C).

At this point, we observe that a_0 , the piston component of the phase, is not determined. But we do not need to be concerned about a_0 . Since all the other terms in the expansion have zero mean, then so will $\phi(x, y)$ without the piston term. Thus, we are assured that our solution will be minimum norm. Furthermore, the normal equations are not ill conditioned,

$$\mathbf{A}^+ \mathbf{A} \mathbf{a} = \mathbf{A}^+ \mathbf{S}, \quad (55)$$

so that we may use the standard least-squares solution

TABLE III. Two-dimensional Legendre polynomials used to represent a wave front $\phi(x,y) = \sum_{k=1}^M a_k n_k F_k(x,y)$ over a square aperture of width D . The constants $g_N = 3(D/2)^2 [1 - 7/(3N^2)]$ and $d_N = (D/2)^2 (1 - 1/N^2)$ are determined such that the polynomials are normalized over a square grid of N^2 sample points.

| k | F_k | n_k^2 | $\frac{\partial F_k}{\partial x}$ | $\frac{\partial F_k}{\partial y}$ |
|-----|-----------------|---|-----------------------------------|-----------------------------------|
| 0 | 1 | 1 | 0 | 0 |
| 1 | x | | 1 | 0 |
| 2 | y | $\frac{3}{d_N}$ | 0 | 1 |
| 3 | $3x^2 - d_N$ | $\frac{5}{3d_N g_N - 5d_N^2}$ | 6x | 0 |
| 4 | $3y^2 - d_N$ | | 0 | 6y |
| 5 | xy | $\frac{9}{d_N^2}$ | y | x |
| 6 | $(3x^2 - d_N)y$ | | 6xy | $3x^2 - d_N$ |
| 7 | $(3y^2 - d_N)x$ | $\frac{15}{3d_N^2 g_N - 5d_N^3}$ | $3y^2 - d_N$ | 6xy |
| 8 | $(5x^2 - g_N)x$ | | 15x^2 - g_N | 0 |
| 9 | $(5y^2 - g_N)y$ | $\frac{7}{6g_N^2 d_N + 25(d_N - g_N)d_N^2}$ | 0 | 15y^2 - g_N |

$$\mathbf{a} = (\mathbf{A}^\dagger \mathbf{A})^{-1} \mathbf{A}^\dagger \mathbf{S}, \quad (56)$$

where $\mathbf{A}^\dagger \mathbf{A}$ is an M by M symmetric matrix, and $\mathbf{A}^\dagger \mathbf{S}$ is a vector of length M whose components are weighted sums (or moments) over the slope data.

From an inspection of the partial derivatives listed in Table III, we note that many of them turn out to be other F_k functions. Thus, those are orthogonal. Fitting data directly to an orthogonal set has the advantage that each may be determined independently by a weighted sum over the data. In terms of Eq. (56), this results in a diagonal $\mathbf{A}^\dagger \mathbf{A}$ matrix. Inversion of a diagonal matrix requires no lengthy numerical procedure. The inverse is also diagonal with the diagonal elements being the reciprocals of corresponding elements.

As an example, suppose we wish to extract all modes up to and including astigmatism, $M = 5$. For $N = 4$ this gives

$$\mathbf{A}^\dagger \mathbf{A} = \begin{pmatrix} 51.2 & 0 & 0 & 0 & 0 \\ 0 & 51.2 & 0 & 0 & 0 \\ 0 & 0 & 32.0 & 0 & 0 \\ 0 & 0 & 0 & 32.0 & 0 \\ 0 & 0 & 0 & 0 & 102.4 \end{pmatrix}. \quad (57)$$

$$\mathbf{A}^\dagger \mathbf{A} = \begin{pmatrix} 51.2 & 0 & 0 & 0 & 0 & 0 & 0 & 145.1 & 0 \\ 0 & 51.2 & 0 & 0 & 0 & 0 & 0 & 0 & 145.1 \\ 0 & 0 & 32.0 & 0 & 0 & 0 & 0 & 0 & 0 \\ 0 & 0 & 0 & 32.0 & 0 & 0 & 0 & 0 & 0 \\ 0 & 0 & 0 & 0 & 102.4 & 0 & 0 & 0 & 0 \\ 0 & 0 & 0 & 0 & 0 & 371.2 & 0 & 0 & 0 \\ 0 & 0 & 0 & 0 & 0 & 0 & 371.2 & 0 & 0 \\ 145.1 & 0 & 0 & 0 & 0 & 0 & 0 & 1691. & 0 \\ 0 & 145.1 & 0 & 0 & 0 & 0 & 0 & 0 & 1691. \end{pmatrix}, \quad (59)$$

$$(\mathbf{A}^\dagger \mathbf{A})^{-1} = \begin{pmatrix} 0.0258 & 0 & 0 & 0 & 0 & 0 & 0 & -0.00211 & 0 \\ 0 & 0.0258 & 0 & 0 & 0 & 0 & 0 & 0 & -0.00211 \\ 0 & 0 & 0.00312 & 0 & 0 & 0 & 0 & 0 & 0 \\ 0 & 0 & 0 & 0.00312 & 0 & 0 & 0 & 0 & 0 \\ 0 & 0 & 0 & 0 & 0.00977 & 0 & 0 & 0 & 0 \\ 0 & 0 & 0 & 0 & 0 & 0.00269 & 0 & 0 & 0 \\ 0 & 0 & 0 & 0 & 0 & 0 & 0.00269 & 0 & 0 \\ -0.00211 & 0 & 0 & 0 & 0 & 0 & 0 & 0.00078 & 0 \\ 0 & -0.00211 & 0 & 0 & 0 & 0 & 0 & 0 & 0.00078 \end{pmatrix} \quad (60)$$

Thus, mode extraction is still numerically fast. For uncoupled modes, they are determined by independent weighted sums of the slope data. For coupled modes, it is a linear combination of the weighted sums for those modes.

MODAL ESTIMATION ERROR

In order to compare the noise propagation properties of modal reconstruction, we next determine the phase error ϵ_i at the discrete grid points, as we did above for the zonal reconstruction. Using Eq. (32) and

$$\mathbf{a} = \mathbf{a}_0 \pm \boldsymbol{\alpha}, \quad (61)$$

where $\boldsymbol{\alpha}$ is the induced random error in the modal coefficients due to the slope measurement noise, we have, from Eq. (49),

$$[\mathbf{A}^\dagger \mathbf{A}]^{-1} = \begin{pmatrix} 0.0195 & 0 & 0 & 0 & 0 \\ 0 & 0.0195 & 0 & 0 & 0 \\ 0 & 0 & 0.0031 & 0 & 0 \\ 0 & 0 & 0 & 0.0031 & 0 \\ 0 & 0 & 0 & 0 & 0.0098 \end{pmatrix}. \quad (58)$$

Furthermore, we note that these matrix elements are not data dependent. They depend only on the sensor geometry such as N . This means they may be fixed, predetermined numbers in Eq. (56). The mode extraction then reduces to a weighted sum over the slope data. In some cases, this sum extends only x - or y -slope data.

Suppose we wish to extract all nine modes shown in Table III. In this case, we note that the derivative of F_8 is not orthogonal to the derivative of F_1 . This leads to an $\mathbf{A}^\dagger \mathbf{A}$ matrix that is no longer diagonal. Fortunately, this is not a serious difficulty. It does not mean we lose the fast mode extraction discussed above for the other modes. In this case the only off-diagonal elements that appear are 1 and 8, and 2 and 9. For the unaffected modes, the inverse is still the reciprocal of the diagonal element. For the modes that are coupled, the inverse is just the inverse of the 2×2 submatrix. Thus, the inverse of $\mathbf{A}^\dagger \mathbf{A}$ is as sparse as $\mathbf{A}^\dagger \mathbf{A}$. To demonstrate this, we write these matrixes for $N = 4$,

$$\epsilon_i = \sum_l \alpha_l n_l F_l(x_i, y_i). \quad (62)$$

Note that ϵ_i automatically has zero mean due to our definition of the F_l functions. Thus, the mean-square phase reconstruction error E is

$$\begin{aligned} E &= \frac{1}{N^2} \sum_i \langle \epsilon_i^2 \rangle \\ &= \sum \langle \alpha_l^2 \rangle = \langle \alpha^+ \alpha \rangle, \end{aligned} \quad (63)$$

where we have used the orthogonality of the F_l functions. We now use Eq. (56) with Eqs. (28) and (61) to obtain α_l

$$\alpha_l = \sum_j [(\mathbf{A}^\dagger \mathbf{A})^{-1} \mathbf{A}^\dagger]_{lj} \sigma_j. \quad (64)$$

This gives from Eq. (63)

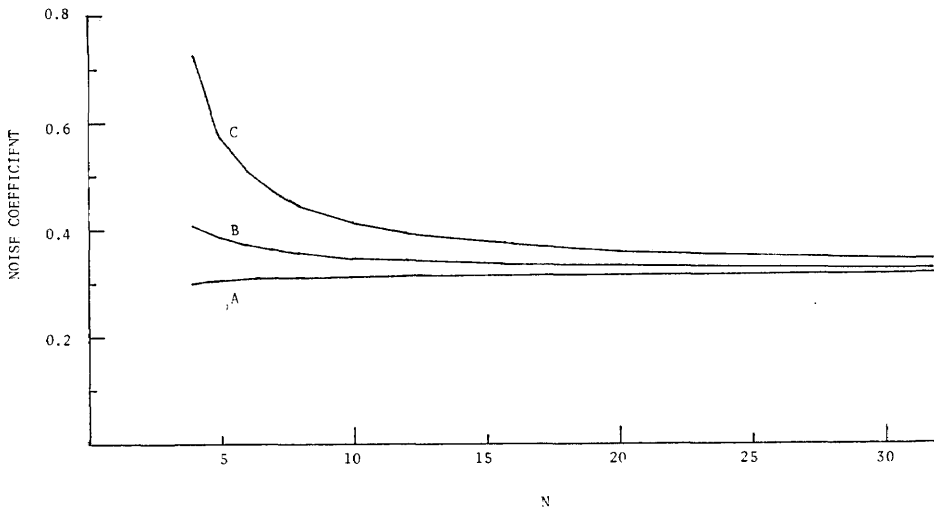


FIG. 3. Noise coefficient for modal estimation versus N for a square array containing N^2 phase points. Curves A, B, and C correspond to the sampling geometries in Fig. 1.

$$E = \sum_l \sum_j \sum_k [(\mathbf{A}^\dagger \mathbf{A})^{-1} \mathbf{A}^\dagger]_{lj} [\mathbf{A}^\dagger (\mathbf{A}^\dagger \mathbf{A})^{-1}]_{kl} \langle \sigma_j \sigma_k \rangle. \quad (65)$$

Ensemble averaging of the slope errors gives

$$\langle \sigma_j \sigma_k \rangle = \sigma^2 \delta_{jk}, \quad (66)$$

where we assume the errors are equal and uncorrelated. Applying Eq. (66) to Eq. (65), we have

$$\begin{aligned} E &= \sum_l \sum_j [(\mathbf{A}^\dagger \mathbf{A})^{-1} \mathbf{A}^\dagger]_{lj} [\mathbf{A} (\mathbf{A}^\dagger \mathbf{A})^{-1}]_{jl} \sigma^2 \\ &= \sum_l [(\mathbf{A}^\dagger \mathbf{A})^{-1} \mathbf{A}^\dagger \mathbf{A} (\mathbf{A}^\dagger \mathbf{A})^{-1}]_{ll} \sigma^2 \\ &= \sigma^2 \sum_l (\mathbf{A}^\dagger \mathbf{A})_{ll}^{-1} = \sigma^2 \text{tr}(\mathbf{A}^\dagger \mathbf{A})^{-1}. \end{aligned} \quad (67)$$

Thus, the mean-square phase error is proportional to the trace of $(\mathbf{A}^\dagger \mathbf{A})^{-1}$, which is the sum of the diagonal elements.

Using our previous definition for C , Eqs. (42) and (47), the error propagation parameter, we have

$$C_{MR} = \frac{1}{h^2} \text{tr}(\mathbf{A}^\dagger \mathbf{A})^{-1}, \quad \text{modal reconstruction}, \quad (68)$$

where h is the distance between sample points.

Equations (58) and (60) give us the breakdown by modes of C_{MR} for $N = 4$, where we can examine the diagonal elements term by term. The data geometry used was as shown in Fig. 1(A).

We evaluated C_{MR} for all data configurations shown in Fig. 1 for several values of N . The results for nine modes are shown in Fig. 3. For small N , like the zonal reconstruction, there is significant difference between the three cases.

The difference may be accounted for by two factors. The first is that the number of data points differs in each case. For Fig. 1(A) we have $2N^2$ slopes, for 1(B) there are $2N(N-1)$, and for 1(C) there are $2(N-1)^2$. The second factor is their location. We note from Fig. 1(C) that we are reconstructing the phase outside the slope sampling region. Phase reconstruction in this region is, like extrapolation, more uncertain.

Cubalchini¹⁰ has also observed that the error propagation depends on the slope geometry (for modal estimation).

DISCUSSION AND CONCLUSIONS

The above explanation may also account for the difference between the zonal reconstruction models of Hudgin and Fried previously reported (and shown as curves B and C in Fig. 2). As might be expected, these differences become smaller as N increases for modal estimation. But for zonal estimation, we note that the differences between the Fig. 1(A) and 2(A) geometries become smaller, but the large gap to Fig. 1(C) geometry (and model) appears to persist even at large N .

We next calculated the mean-square phase error as before, using the sum of the solutions with separate unity slopes, except that this time we weighted the outer zones by one-half and the corners by one-fourth. This was also done by Fried.⁴ Essentially this reduces the size of the aperture such that the outer phase points lie on the boundary. The results are shown in Fig. 4. All three configurations improved, but Fig. 1(C)

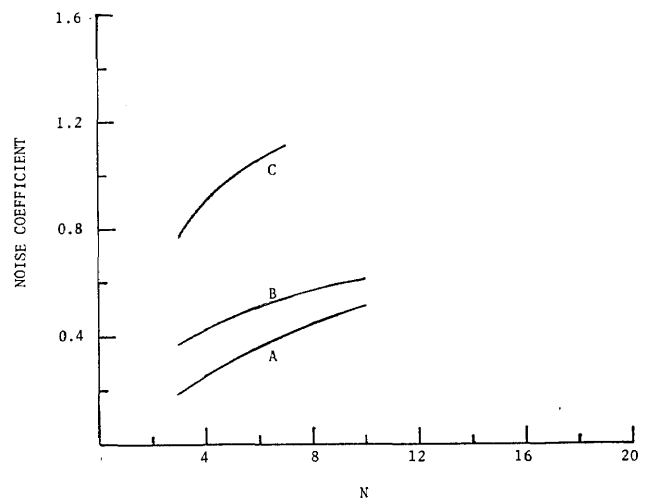


FIG. 4. Noise coefficient for zonal estimation on a reduced aperture. The phase reconstruction error was evaluated as in Fig. 2, except that the perimeter points are weighted by one-half and the corners by one-fourth.

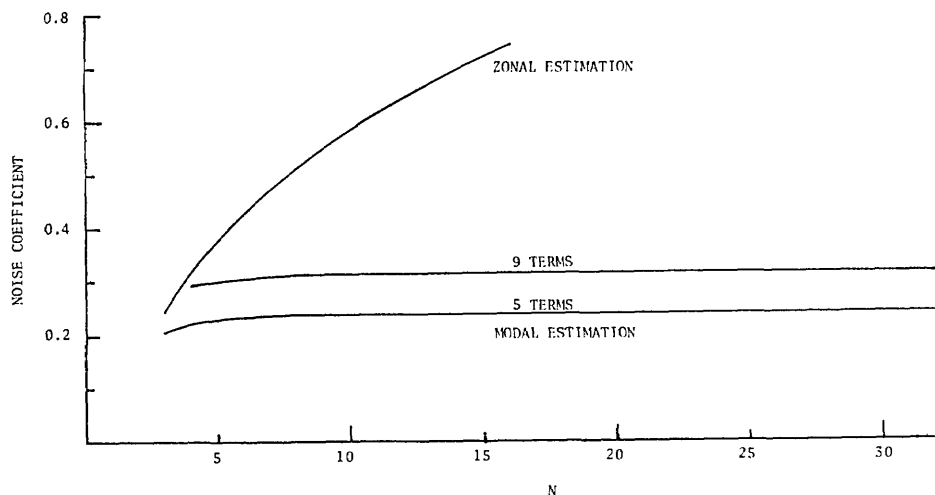


FIG. 5. Noise coefficient comparison between zonal estimation and modal estimation. The slope geometry used was Fig. 1, configuration A.

improved the most, although there is still a significant gap that appears to persist at large N . However, from Fig. 1, we see that even for the reduced aperture, Fig. 1(C) geometry still has no slope data on the boundary. This, at least, partially explains the gap at small N . Nevertheless, for coincident x - and y -slope geometry, Fig. 1(A) and its associated slope model, Eqs. (9) and (10) produce significantly less phase error than the geometry of Fig. 1(C) and Eqs. (7) and (8).

We next compared the noise coefficient obtained by using zonal or modal estimation models. The comparison is plotted in Fig. 5. We note that generally the modal error depends on the number of modes being extracted from the data. Modal estimation appears to be superior to zonal estimation, especially when only a fixed number of modes are of interest. Furthermore, we have shown that modal estimation is computationally easier and faster. And, finally, both of these advantages for modal estimation, noise propagation, and computational difficulty are enhanced as N increases.

- ¹K. T. Knox, "Image retrieval from astronomical speckle patterns," *J. Opt. Soc. Am.* **66**, 1236-1239 (1976).
- ²M. P. Rimmer, "Methods for evaluating lateral shearing interferograms," *Appl. Opt.* **13**, 623-629 (1974).
- ³R. H. Hudgin, "Wave-front reconstruction for compensated imaging," *J. Opt. Soc. Am.* **67**, 375-378 (1977).
- ⁴D. L. Fried, "Least-square fitting of a wave-front distortion estimate to an array of phase-difference measurements," *J. Opt. Soc. Am.* **67**, 370-375 (1977).
- ⁵R. J. Noll, "Phase estimates from slope-type wave-front sensors," *J. Opt. Soc. Am.* **68**, 139-140 (1978).
- ⁶B. R. Hunt, "Matrix formulation of the reconstruction of phase values from phase differences," *J. Opt. Soc. Am.* **69**, 393-399 (1979).
- ⁷R. L. Frost, C. K. Rushforth, and B. S. Baxter, "Fast FFT-based algorithm for phase estimation in speckle imaging," *Appl. Opt.* **18**, 2056-2061 (1979).
- ⁸J. Herrmann, "Least-squares wave-front errors of minimum norm," *J. Opt. Soc. Am.* **70**, 28-35 (1980).
- ⁹D. M. Young, *Iterative Solutions of Large Linear Systems* (Academic, New York, 1972).
- ¹⁰R. Cubalchini, "Modal wave-front estimation from phase derivative measurements," *J. Opt. Soc. Am.* **69**, 972-977 (1979).